Hydroxyapatites: Key Structural Questions and Answers from Dynamic Nuclear Polarization

César Leroy, Fabien Aussenac, Laure Bonhomme-Coury, Akiyoshi Osaka, Satoshi Hayakawa, Florence Babonneau, Cristina Coelho-Diogo, Christian Bonhomme

Article

Hydroxyapatites: Key Structural Questions and Answers from DNP (Dynamic Nuclear Polarization)

Cesar Leroy, Fabien Aussenac, Laure Bonhomme-Coury, Akiyoshi OSAKA, Satoshi Hayakawa, Florence Babonneau, Cristina Coelho Diogo, and Christian Bonhomme

Anal. Chem., **Just Accepted Manuscript** • DOI: 10.1021/acs.analchem.7b01332 • Publication Date (Web): 05 Sep 2017

Hydroxyapatites: Key Structural Questions and Answers from DNP (Dynamic Nuclear Polarization)

César Leroy[1], Fabien Aussenac[2], Laure Bonhomme-Coury[1], Akiyoshi Osaka[3], Satoshi Hayakawa[3], Florence Babonneau[1], Cristina Coelho-Diogo[4] and Christian Bonhomme[1]*

[1]Sorbonne Universités, UPMC Univ Paris 06, CNRS, Collège de France, Laboratoire de Chimie de la Matière Condensée de Paris (LCMCP), 4 Place Jussieu, 75252 Paris Cedex 05, France, [2]Bruker France, 34, rue de l'Industrie, 67166 Wissembourg, France, [3]Graduate School of Natural Science and Technology, University of Okayama, Okayama, Japan, [4]Sorbonne Universités, UPMC Univ Paris 06, CNRS, Institut des Matériaux de Paris Centre (IMPC-UPMC-FR2482), 75252 Paris, Cedex 05 France.

ABSTRACT: We demonstrate that NMR/DNP (Dynamic Nuclear Polarization) allows an unprecedented description of carbonate substituted hydroxyapatite (CHAp). Key structural questions related to order/disorder and clustering of carbonates are tackled by using distance sensitive DNP experiments using ^{13}C-^{13}C recoupling. Such experiments are easily implemented due to unprecedented DNP gain (orders of magnitude). DNP is efficiently mediated by quasi one-dimensional spin diffusion through the hydroxyl columns present in the CHAp structure (thought as "highways" for spin diffusion). For spherical nanoparticles and $\varnothing < 100$ nm, it is numerically shown that spin diffusion allows their study as a whole. Most importantly, we demonstrate also that the DNP study at 100 K leads to data which are comparable to data obtained at room temperature (in terms of spin dynamics and lineshape resolution). Finally, all 2D DNP experiments can be interpreted in terms of domains exhibiting well identified types of substitution: local order and carbonate clustering are clearly favored.

INTRODUCTION

Nanosized substituted hydroxyapatite (HAp) is a fundamental mineral in nature, as it represents the key mineral architecture in bone, dentin and enamel (*biological* apatites)[1,2]. Moreover, *synthetic* substituted HAp (including *carbonated* HAp, CHAp) is extensively used in medicine and dentistry due to its exceptional bioactivity and biocompatibility properties[3]. Despite numerous physicochemical analyses (X-ray and neutron diffraction, vibrational spectroscopies, thermal analyses…), the structural description of substituted apatites remains largely hypothetical and particularly challenging. Focusing on the particular case of carbonate substitution, Leventouri[4] stressed a fundamental crystal structure problem related to the precise location of carbonates in CHAp known as the "carbonate substitution problem"[5,6] in A (OH^-) and/or B (PO_4^{3-}) sites. Quoting Ren *et al.* in 2014[7]:

"*Due to very limited information on direct structural analysis of carbonated HAp quality single crystals, the exact location of* CO_3^{2-} *in apatite is still a mystery*".

Two fundamental questions can be raised, namely (i) the notion of *order/disorder* in CHAp, (ii) the potential *clustering* of the substituted anions/cations in HAp. To tackle such questions, XRD and FTIR suffer from major drawbacks, *i.e.* the long range order averaged description of the atomic positions, and the very local description of chemical groups, respectively. Theoretically, the ability of solid state NMR to establish *through space connectivities* should fill the gap between very local properties and long-range order features. Apart from sensitive nuclei (^1H, ^{31}P)[8,9,10,11,12,13,14,15], all other nuclei present as substitutions suffer from severe sensitivity limitations due to low natural abundance (^{13}C, 1.1%) *and/or* intrinsic low wt%[16,17]. It precluded so far the routine use of dipolar based triple resonance experiments (^1H–X–Y; X, Y = ^{13}C, ^{31}P…) which should probe the spatial distribution even in the case of partially disordered materials.

To circumvent this limitation, Dynamic Nuclear Polarization (DNP) was implemented here for the first time, following the work of Griffin *et al.*[18]. DNP corresponds to the efficient transfer of polarization at low temperature (~ 100 K) from unpaired electrons (present in radicals or biradicals such as TOTAPOL[19] or AMUPol[20]) to NMR active nuclei. The gain in notoriety of DNP is associated to very large gain in sensitivity (*several orders in magnitude*) and impressive applications for low abundant nuclei[21,22,23,24,25,26,27,28,29,30,31,32,33,34,35].

In this contribution, we claim that DNP opens new avenues for unprecedented characterization of CHAp and

allows answering the key questions raised above (points (i) and (ii)). The proposed methodology can be extended to all types of substitutions, as soon as one NMR active nucleus is present. In the case of CHAp nanoparticles, DNP and proton spin diffusion (SD) allow the global characterization of a given nanoparticle, including its surface *and* core. We estimate the limit diameter for which the core contribution will be underestimated during the DNP/SD process to ~ 500 nm. The DNP efficiency allows recording 2D triple resonance experiments within an hour (instead of days or even months). Full assignments of the NMR lines are proposed, as well as very first realistic schemes for the substitutions. We mention here that CHAp nanoparticles have been studied recently in the frame of ^{1}H-^{43}Ca DNP CP MAS experiments[36]. It has been claimed that such technique was suitable for site selection (CHAp nanoparticle surface *vs* core species). We stress here that such selection is by no means related to the SENS acceptance[21] of DNP, namely Surface Enhanced NMR Spectroscopy. Due to the very large DNP enhancements (using glycerol in [36]), 2D ^{1}H-^{43}Ca DNP HETCOR experiments were implemented leading to the observation of clear correlations between ^{43}Ca nuclei and OH^- species (located in the columns) and protons belonging to the solvent. Such correlations were attributed to *distinct* species without particular selectivity. It has to be mentioned that the use of glycerol adds complexity in terms of chemistry (chemical bonding, potential partial dissolution) and spin dynamics. The study presented below is by far more simple as D_2O/H_2O is used as DNP solvent.

All in all, the DNP approach unifies standard characterizations (including diffraction and vibrational methods)[2,4,5,37], theoretical modeling of CHAp structures[38,39,40] and breaks the barriers in understanding the CHAp structure.

RESULTS AND DISCUSSION

CHAp: a prototype for DNP and one-dimensional ^{1}H–^{1}H spin diffusion (SD). The fundamental feature of CHAp is the presence of OH^- columns parallel to the *c*-axis (Figure 1a). It follows that *one-dimensional* ^{1}H SD can be considered as a reasonable approximation. Taking into account the structural characteristics of HAp, the diffusivity, D, along the channels is estimated to D ~ 0.5 $nm^2.ms^{-1}$ (see Supporting information). The protons in close contact with the surface of the nanoparticles are first DNP polarized (Figure 1b). Protons located in the core of the nanoparticles are subsequently polarized by SD.[41,42,43,44,45] We demonstrate unambiguously that in the case of nanoparticles of ∅ ~ 30 nm (Figure S1), *all protons* are indeed polarized. This assumption still holds under moderated MAS conditions (ν_{rot} = 8 kHz) (see Supporting information).

DNP enhancement for synthetic CHAp nanoparticles: 1D and 2D ^{31}P–^{13}C and ^{13}C–^{13}C distance sensitive experiments. The syntheses of ^{13}C labeled (CHAp) and natural abundance (*n.a.*CHAp) samples are presented in the Experimental section, as well as the sample preparation for DNP experiments. Figure 2 shows the DNP efficiency for ^{1}H, ^{31}P and ^{13}C (CHAp). The DNP enhancement is further increased by using AMUPol instead of TOTAPOL and reached ε ~ 23 for all observed nuclei. The reduction in experimental time can be roughly estimated by ε^2 ~ 550. The ^{1}H → ^{31}P DNP spectrum is characteristic for a substituted HAp ($\delta_{iso}(^{31}P)$ ~ 3.0 ppm) and exhibits a broadening of the line when compared to pure HAp[12]. The content in HPO_4^{2-} is negligible[10,13] as demonstrated by 2D ^{1}H → ^{31}P HETCOR CP MAS experiments implemented at room temperature (RT) (Figure S2). Remarkably, the ^{13}C resolution is clearly sufficient to distinguish both A and B sites contributions (four main isotropic ^{13}C resonances) and comparable to the one observed using standard NMR at RT (Figure S3). Moreover, the CP dynamics is comparable, both at 100 K and RT (Figure S4). The detailed analyses of the variable contact time curves showed also that no HCO_3^- species were involved (Figure S5)[17]. *It follows that the DNP data obtained at ~ 100 K can be safely compared to those obtained at RT and that the conclusions derived from the DNP methodology are indeed representative of CHAp.*

^{1}H → ^{31}P → ^{13}C DNP double CP MAS experiments were successfully implemented (Figure 3a, black line) in a very short experimental time (~ 3 min.). In the particular case of CHAp, only double resonance experiments (^{1}H→ ^{13}C) were proposed so far in the literature for ^{13}C labeled samples[17]. In Figure 3b, the corresponding 2D HETCOR experiment (obtained in less than 4 hours) is presented. Each ^{13}C resonance is individually connected to ^{31}P components which are slightly different in terms of $\delta_{iso}(^{31}P)$. Moreover, a fraction of B sites is slightly correlated to a deshielded component of the ^{31}P spectrum ($\delta_{iso}{}^{31}P$ ~ 5.6 ppm). The DNP efficiency was sufficient to implement the same experiment for *n.a.*CHAp (Figure S6, ~ 10 hours) leading to very comparable information. Such experiment would have been impossible to implement using standard NMR at room temperature!

Finally, ^{1}H → ^{13}C → ^{13}C DNP MAS experiments based on double quantum (DQ) dipolar recoupling[46] were successfully implemented (Figure 3c, ~ 7 hours). In principle, such a sequence should highlight spatial connectivities between the carbonate groups. Despite the very small $\delta_{iso}(^{13}C)$ chemical shift range (~ 5 ppm), a remarkable resolution is obtained in both dimensions. Several *off*-diagonal correlations are observed (for instance at $\delta_{iso}(^{13}C)_{B/B}$ = 170.1 and 171.0 ppm) (^{13}C sites exhibiting *different chemical environments*) as well as *on*-diagonal correlation ($\delta_{iso}(^{13}C)_{B/B}$ = 168.3 ppm) (*same chemical environment*). We recall here that the amount of carbonates is very small (roughly 5 wt%) and that ^{13}C labeling is therefore mandatory for the implementation of the ^{13}C DQ experiments.

Towards a definitive picture of carbonates in CHAp. The goal of this last section is to derive realistic CHAp

models from the set of DNP data described above. Considering the connectivities between carbonates, Figure 3c is the most informative. The clear observation of *at least* nine individual ^{13}C correlations (shown by arrows) in a ~ 5 ppm shift range proves that *local order is definitely present* (leading to well defined chemical environment for each ^{13}C nucleus) (see also Figure S7 and the Experimental section). The slices in Figure 3c are presented without any GB treatment in order to avoid the presence of artefacts. We have checked that the indirect chemical shifts for i), ii), iii) and iv) correspond to the sums of the involved (direct) chemical shifts (Figure S7). Charge compensation is the key concept and several authors have proposed the following favorable replacement schemes (based on experimental observations[2,4,5,7,37] and energy minimization[38,39,40]):

(1) A substitution: $CO_3^{2-} = 2\ OH^-$

(2) A/B substitution: $2\ CO_3^{2-} = OH^- + PO_4^{3-}$

(3) B/B substitution: $\square_{Ca2+} + 2\ CO_3^{2-} = Ca^{2+} + 2\ PO_4^{3-}$

We use here Fleet's notations2 showing the substituting constituents on the left hand side of the equation. We neglect a forth possible scheme (B substitution), $Na^+ + CO_3^{2-} = Ca^{2+} + PO_4^{3-}$, as the Na wt% is small (see the Experimental section).

At first sight, the multiplicity of B/B contributions (eq. (3)) in Figure 3c is complex to analyze and needs some invention at this point. Indeed, strong (*off*-diagonal) and much less intense (*off*- and *on*-diagonal) correlations are observed (*vide supra*). We assume first that correlations correspond to the shortest distances between ^{13}C sites. In pure HAp (Figure 4a), the *shortest* $d_{(P-P)}$ distances (~ 4.0 Å) are found in zig-zag chains with overall *c*-axis direction: B/B association corresponds to *consecutive* positions in a given chain. Considering a *single* B/B group (C_1/C_2, Figure 4b, left) in $Ca_{19}(PO_4)_{10}(CO_3)_{2(B/B)}(OH)_4$ (wt%(CO_3^{2-}) = 6.3 %), a vacancy ($\square_{Ca2+}$) is present near one of the carbonate, leading consequently to $\delta_{iso}(^{13}C_1) \neq \delta_{iso}(^{13}C_2)$ and *off*-diagonal correlations in the ^{13}C DQ spectrum. We assign the intense correlations at $\delta_{iso}(^{13}C)_{B/B}$ = 170.1 and 171.0 ppm to such B/B groups. At this stage, the main challenge is to safely assign the less intense correlations. The *on*-diagonal correlation located at $\delta_{iso}(^{13}C)_{B/B}$ = 168.3 ppm indicates that some carbonates must have somehow *equivalent chemical environments* (and the same chemical shifts), in clear contradiction with B/B association described just above (as $\delta_{iso}(^{13}C_1) \neq \delta_{iso}(^{13}C_2)$, necessarily!). This intriguing fact can be explained as follows.

Consider now four carbonates (C_i, i: 1 → 4) and two associated $\square_{Ca2+}$ along a given zig-zag chain, as shown in Figure 4b, right (HAp supercell, $Ca_{38}(PO_4)_{20}(CO_3)_{4(B/B)}(OH)_8$, with wt%($CO_3^{2-}$) = 6.3 %). The relative location of $\square_{Ca2+}$ implies C_4^2 = 6 distinct configurations. We suppose that $\delta_{iso}(^{13}C_i)$ is mainly dominated by the effect of the *first* neighbors along the zig-zag chain. It follows that 8 distinct $\delta_{iso}(^{13}C_i) \equiv \delta_m$ (m: 1 → 8) can be expected. In other words, a given $^{13}C_i$ (Figure 4b, right) can be characterized by several δ_m. Taking into account all connectivities between consecutive $^{13}C_i$ (δ_m) and $^{13}C_{j\neq i}$ ($\delta_{m'}$) lead to a correlation map (Figure 4c) exhibiting *both on*- and *off*-diagonal correlations, in agreement with DQ data (at least qualitatively). This simple approach is further discussed in Figure S8 for potential correlations corresponding to longer ^{13}C–^{13}C distances.

Finally, one notes the absence of *on*-diagonal A/A correlations whereas *off*-diagonal A/B correlations ($\delta_{iso}(^{13}C)_{\underline{A}/B}$ = 166.5 ppm, $\delta_{iso}(^{13}C)_{A/\underline{B}}$ = 168.0 ppm) are clearly evidenced. This result unambiguously reveals A/B substitutions (eq. (2)) in absence of A/A associations (eq. (1)). Moreover, as $d_{(^{13}C-^{13}C)}$ ~ 3.90 – 4.02 Å in A/B associations[38], it is concluded that the DQ experiment is effectively sensitive to $d_{(^{13}C-^{13}C)}$ distances up to ~ 4.0 Å (at least) as presupposed in the analysis of B/B correlations (*vide supra*). The A/B association can be represented by a supercell of formula $Ca_{20}(PO_4)_{11}(CO_3)_{2(A/B)}(OH)_3$[38] (wt%($CO_3^{2-}$) = 5.9 %, a value comparable to the experimental one).

However, DQ experiments are not sensitive to potential *isolated* A and/or B sites and therefore are not relevant to evidence their presence/absence. In the structure of A type CHAp[38], each *isolated* A site is surrounded by six PO_4^{3-} groups involving $d_{(^{13}C-^{31}P)}$ ~ 3.89 – 4.09 Å (instead of two or three PO_4^{3-} for B and A/B sites). It follows that *isolated* A sites should be specifically overestimated by $^{31}P \rightarrow {}^{13}C$ CP transfer. Obviously, this is not the case experimentally (Figure 3a), suggesting that A sites are mostly present in A/B combination. On the other hand, ^{31}P filtering leads to a slight overestimation of the resonance at $\delta_{iso}(^{13}C)$ ~ 170.2 ppm. This can be assigned to *isolated* B sites having more PO_4^{3-} neighbors than *clustered* B sites (*vide supra* and Figure 4b). These particular B sites are slightly correlated to a characteristic deshielded component of the ^{31}P spectrum ($\delta_{iso}(^{31}P)$ ~ 5.6 ppm) (Figure 3b)[47].

All in all, CHAp nanoparticles can be safely understood as domains corresponding to *clustered* B/B ($Ca_{19}(PO_4)_{10}(CO_3)_{2(B/B)}(OH)_4$ and $Ca_{38}(PO_4)_{20}(CO_3)_{4(B/B)}(OH)_8$) substitution (major contribution), A/B ($Ca_{20}(PO_4)_{11}(CO_3)_{2(A/B)}(OH)_3$) substitution (minor contribution), and a fraction of isolated B sites.

EXPERIMENTAL SECTION

Syntheses of samples. n.a.CHAp: all experiments were conducted in a glovebox under flowing dry N_2 gas. Standard precipitation of CHAp in aqueous solution (at room temperature) was performed. All solutions were first decarbonated (boiling them and using an argon flux during the syntheses). A solution of ammonium hydrogenphosphate ($(NH_4)_2HPO_4$, 0.30 mol.L^{-1}, pH ~ 10) was added to a solution of calcium nitrate tetrahydrate ($Ca(NO_3)_2.4H_2O$,

0.50 mol.L^{-1}, pH ~ 5) using a titration apparatus (808 Titrando, Methrom, 3 mL.min^{-1}). Carbonates were introduced by adding sodium hydrogencarbonate ($NaHCO_3$) to the phosphate solution. All experiments were performed under argon flux and magnetic stirring. The initial molar ratios were: Ca: 10, P: 6, CO_3^{2-}: 3. After the addition of the phosphate solution, the obtained precipitates were further stirred for 24 hours. After centrifugation, the precipitates were rinsed 4 times with distilled water (final pH of water ~ 7). All samples were then heat treated (400°C) for 48 hours in order to eliminate remaining water and ammonia molecules. Elemental analyses: performed at the Centre d'Analyses CNRS, Vernaison, France. Found wt%: Ca: 34.17, P: 15.66, C: 1.04, Na: 0.33, N: 1.23. CO_3^{2-} wt%: 5.20. CHAp: basically, the same protocol used for n.a.CHAp was implemented, using $NaH^{13}CO_3$ (fully labeled in ^{13}C) as a source of carbonates. The same sample treatment (stirring, centrifugation, rinsing, heating at 400°C for 48 hours) was implemented. Found wt%: Ca: 37.60, P: 17.01, C: 0.97, Na: 0.35, N: <0.10. CO_3^{2-} wt%: 4.80. Routine characterization (XRD, FTIR) of n.a.CHAp and CHAp are presented in Figures S9 and S10.

Solid-state DNP/NMR experiments. Sample preparation for n.a.CHAp and CHAp: the TOTAPOL[19] and AMUPol[20] biradical polarizing agents were used in $D_2O(90)/H_2O(10)$ solutions. For TOTAPOL: 2.4 mg were dissolved in 270 µL of D2O and 30 µL of H2O leading to a 20.0 mM.L^{-1} TOTAPOL solution. ~ 30 mg of sample of interest was impregnated with 15 µL of the corresponding TOTAPOL solution. The mixture was then inserted in a 3.2 mm sapphire rotor and rapidly cooled down to ~ 100 K. The mass of sample of interest in the rotor was estimated to ~ 15 mg. For AMUPol: 1.1 mg were dissolved in 90 µL of D_2O and 10 µL of H_2O leading to a 15.0 mM.L^{-1} AMUPol solution. ~ 30 mg of sample of interest was impregnated with 15 µL of the corresponding AMUPol solution. Glycerol (glass former) was not used in this study. DNP/NMR: all DNP MAS experiments were recorded using a Bruker DNP-NMR AVANCE III 400 MHz spectrometer equipped with a gyrotron and associated transmission line capable of delivering more than 5 W of ~ 263 GHz microwave irradiation at the sample. All experiments were recorded with a 3.2 mm HXY triple-resonance MAS probe at $\nu_0(^1H)$ = 400.07 MHz corresponding to the maximum ^1H enhancement field position for AMUPol at $\nu_0(e^-)$ = 263.5 GHz, with the X-channel tuned to $\nu_0(^{31}P)$ = 161.95 MHz and the Y-channel tuned to $\nu_0(^{13}C)$ = 100.60 MHz. The MAS rotation frequency was systematically fixed at 8 kHz. The ε factor was measured for ^1H by recording ON and OFF experiments (single pulse experiment, SPE or spin echoes to avoid baseline distortions). ε was measured independently for the solvent resonance and for the OH^- resonance of the apatitic structures. $^1H(\pi/2)$ = 2.7 µs (92.5 kHz). Systematic measurements of $T_1(^1H)$ were performed (saturation-recovery) in order to anticipate the relaxation delay in ^1H–X DNP CP MAS experiments (~ 1.3 T1). The collector current was optimized keeping in mind the corresponding increase of temperature of the sample during the ON experiments: ~ + 6 K for c.a. 5 W microwave irradiation at the sample. Hartmann-Hahn double (and triple) resonance profiles for ^{31}P and ^{13}C were recorded using CHAp as a model compound. For ^{31}P and ^{13}C, ramped spin locking[48] was implemented to facilitate the CP transfer under MAS. SPINAL-64[49] was used for heteronuclear decoupling. The intensity of the signals was optimized by recording variable contact time experiments. For triple resonance experiments, a double CP transfer was implemented. Systematic control experiments were performed in order to prove the absence of any Zeeman contribution to the observed signals. 2D HETCOR CP MAS experiments were recorded under ^1H homonuclear decoupling using the Frequency Switched Lee-Goldburg (FSLG) scheme[50]. In the case of the ^{13}C-^{13}C recoupling experiment under MAS, the SPC5 scheme[46] was implemented (with $^1H \rightarrow {}^{13}C$ CP MAS transfer prior to the recoupling pulses). Again, CHAp was used for the set-up of the experiments: RF power on the ^{13}C channel and the number of recoupling loops were carefully optimized (4 ms). The application of GB (Gaussian multiplication) apodization was carefully checked on both dimensions in order to clearly distinguish signals from wiggles. In order to strengthen that at least nine individual ^{13}C correlations are indeed observed, a non-windowed 2D-FT plot is presented in Figure S7. One clearly notes that the extracted slices (noted **i)** to **iv)**) are fully comparable to those observed in Figure 3c (with GB apodization). In other words, the wiggles present in Figure 3c are not inducing deleterious distortions of the 2D spectrum. The NMR parameters used are the following. Figure 2a. NS (number of scans) = 4, relaxation delay = 8.5 s, experimental time ~ 30 s. Figure 2b. NS = 16, relaxation delay = 8.5 s, contact time = 9 ms, experimental time ~ 2 min. Figure 2c. NS = 16, relaxation delay = 8.5 s, contact time = 9 ms, experimental time ~ 2 min. Figure 3a. Red spectrum: NS = 16, relaxation delay = 8.5 s, contact time = 9 ms, experimental time ~ 2 min. Black spectrum: NS = 16, relaxation delay = 6.5 s, contact time = 9 ms and 20 ms, experimental time ~ 2 min. Figure 3b. NS = 16, relaxation delay = 8.5 s, number of t_1 increments: 96, contact time = 9 ms and 20 ms, experimental time ~ 3h40min. Figure 3c. NS = 32, relaxation delay = 8.5 s, number of t_1 increments: 96, experimental time ~ 7h.

CONCLUSION

In this contribution, we have clearly demonstrated that DNP is suitable for unprecedented description of substitutions in hydroxyapatite nanoparticles. The DNP gains are sufficient to implement dipolar based experiments which would have been impossible to set up using standard NMR conditions. The DNP approach is fully complementary to standard XRD and FTIR analyses as it allows the description of the substituants at an *intermediate order range*. The approach is general (in terms of efficient DNP solvent, biradical and sample preparation) and can be applied to all types of substitution as soon as one NMR active nucleus is present. Very interestingly, hydroxyap-

atite is a prototype structure for DNP as *quasi* one-dimensional proton spin diffusion is still active under moderate MAS and allows the description of a nanoparticle in its entirety. We have answered to two main structural questions regarding CHAp, namely the presence of local order and the clustering of carbonates. Most importantly, we have shown that: (i) the DNP approach can be easily extended to natural abundance (^{13}C) samples, (ii) DNP is obviously suitable for the study of natural nano-crystals such as those found in bones and teeth as their characteristic dimensions are much smaller than 100 nm, (iii) the DNP derived structural models will act as valuable starting point for first principles calculations of NMR parameters and further independent validation.

CAPTION OF FIGURES

Figure 1. a) Schematic representation of pure HAp (here in the monoclinic form). O: red, H: black, Ca: blue, P: green. The same colour is used for all positions of a given atom (3 for P, 5 for Ca, 1 for H and 13 for O). A sites correspond to OH^- whereas B sites correspond to PO_4^{3-} groups. The OH^- columns are represented schematically by cylinders (parallel to the *c*-axis). **b)** Simplified description of DNP process and ^1H–^1H spin diffusion (SD) along the OH^- columns. In a first approximation, SD can be considered as *one-dimensional* ($D_{H\text{-}H}^{intra}$ ~ 3.0 kHz): H_2 is essentially coupled to H_1 and H_3 and so on for increasing n. Columns are well separated ($D_{H\text{-}H}^{inter}$ ~ 0.2 kHz). The numerical estimations of Ω (transition rate) and D (diffusivity) are presented in Supporting information. In energetically relaxed models[38], O–H–O angle are *approximately* 180° (but can be slightly different). Black triangles correspond to carbonate groups in A/B sites: adjacent OH^- groups are rotated almost perpendicular to the *c*-axis[38]. L ~ 300 Å corresponds to the longest chain of OH^- in CHAp nanoparticles of ∅ ~ 30 nm. Grey ovals: surface of the corresponding nanoparticle and {solvent + biradicals} ($D_2O(90)/H_2O(10)$, TOTAPOL or AMUPol – see the Experimental section). The saturation of the EPR transitions of the biradicals by Microwave (MW) leads to efficient DNP transfer to the protons of the columns through cross effect (CE).

Figure 2. a) ^1H DNP MAS spectrum of CHAp (T ~ 100 K). OFF (without microwave, MW) and ON (with MW) spectra are presented for TOTAPOL and AMUPol. ε(^1H) corresponds to the ratio ON/OFF[18]. S: DNP solvent. Protons of CHAp are located at 0.0 ppm (OH^-). ε(^1H) for the OH^- resonance is comparable to the one of the solvent. **b)** $^1H \rightarrow {}^{31}P$ DNP CP MAS spectrum of CHAp. Insert: the ON and OFF spectra are strictly comparable. **c)** $^1H \rightarrow {}^{13}C$ DNP CP MAS spectrum of CHAp. Insert: ^{13}C spectral resolution and ^{13}C ranges for A,B carbonates. Typical experimental time is given for each nucleus (in s or min.). *: spinning sidebands.

Figure 3. a) $^1H \rightarrow {}^{13}C$ (red) and $^1H \rightarrow {}^{31}P \rightarrow {}^{13}C$ (black) DNP CP MAS spectra of CHAp (with AMUPol). Spectra were obtained in 2 and 3 min., respectively. In grey: MW OFF. **b)** $^1H \rightarrow {}^{31}P \rightarrow {}^{13}C$ DNP HETCOR CP MAS spectrum of CHAp. Dashed lines are guidelines for the eyes. **c)** $^1H \rightarrow {}^{13}C \rightarrow {}^{13}C$ DNP DQ CP MAS (SPC5) spectrum of CHAp[46]. Particular slices (noted **i)** → **iv)**) are highlighted on the right of the Figure. A and B ^{13}C resonance ranges are indicated[16] in orange and violet, respectively. The 2D experiment is presented with GB (see the Experimental section) whereas the slices are presented with standard FT (no GB). Vertical black arrows: ^{13}C correlations (A and B sites).

Figure 4. a) Pure HAp (monoclinic form). The *c*-axis is vertical (black double-arrow). As soon as CO_3^{2-} groups are inserted, structures with P1 space group are basically considered[38]. O: red, H: black, Ca: blue, P: green. The same colour is used for all positions of a given atom, for example green for P1, P2 and P3 (see also Figure 1a). All O atoms are omitted for clarity except those corresponding to OH^- groups. The Pi–Pi (i = 1, 2, 3) zig-zag chains are in the main direction of the *c*-acis (green double-arrows). $d_{(Pi-Pi)}$ < 4.2 Å and (Pi–Pi–Pi) ~ 113°. **b)** Several schemes corresponding to B/B associations exhibiting $d_{(Pi-Pi)}$ < 4.2 Å (all Ca atoms are omitted for clarity). The vertical black dashed line is a guideline for the eye to separate the left and right parts of the Figure (see main text). Left: two B sites corresponding to: $\square_{Ca2+} + 2\ CO_3^{2-} = Ca^{2+} + 2\ PO_4^{3-}$ (eq. (3) in the main text). ● and ▣ correspond to a CO_3^{2-} group, and a CO_3^{2-} group "associated" to a Ca^{2+} vacancy ($\square_{Ca2+}$), respectively. Right: six (C_4^2) possible configurations corresponding to four CO_3^{2-} and two associated Ca^{2+} vacancies ($2\ \square_{Ca2+} + 4\ CO_3^{2-} = 2\ Ca^{2+} + 4\ PO_4^{3-}$). The six chains are located nearby for clarity. For a given chain: the four carbonates are labeled C_i (i: 1 → 4). We make the following assumption: $\delta_{iso}(^{13}C_i) \equiv \delta_m$ (m: 1 → 8) is mainly dominated by the effect of the first neighbors along the given zig-zag chain, *i.e.* P, CO_3^{2-} (●) or CO_3^{2-} associated to a Ca^{2+} vacancy (▣). As examples: ● linked to {P, ▣} is named δ_3; ● linked to {●, ▣} is named δ_5. Taking into account all six configurations, eight *a priori* different $\delta_{iso}(^{13}C)$ are evidenced (noted δ_i, i = 1 → 8). **c)** Theoretical dipolar ^{13}C–^{13}C correlation map associated to the six configurations and based on carbonates located on *consecutive* positions in the zig-zag chains. *On*-diagonal correlations are underlined in blue. As examples: δ_3 is linked to δ_4 in a zig-zag chain leading to {δ_3,δ_4} *off*-diagonal × in the correlation map ; δ_4 is linked to $\delta_{2,3,4,5}$ in the zig-zag chains leading to {δ_4,$\delta_{2,3,5}$} *off*-diagonal × and {δ_4,δ_4} *on*-diagonal × in the correlation map.

FIGURE 1

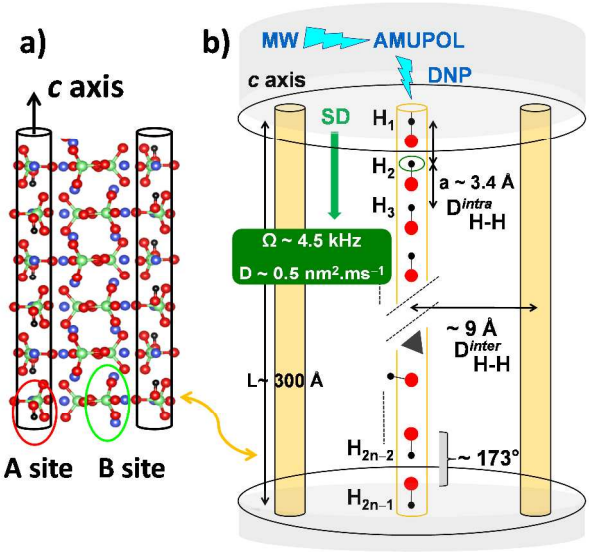

FIGURE 2

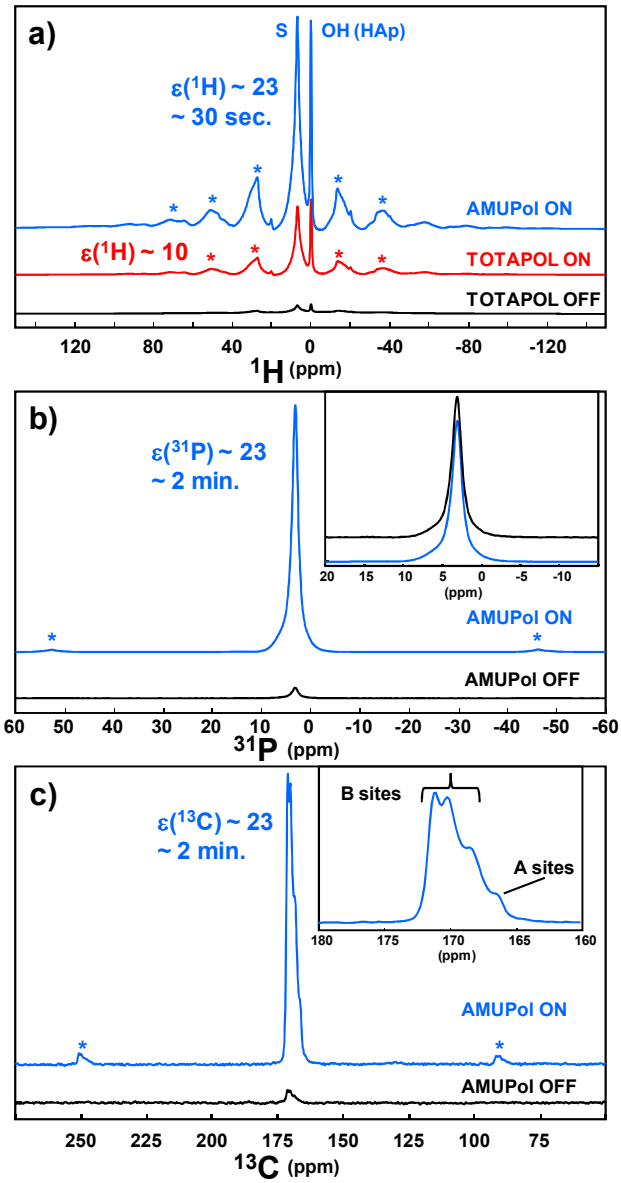

FIGURE 3

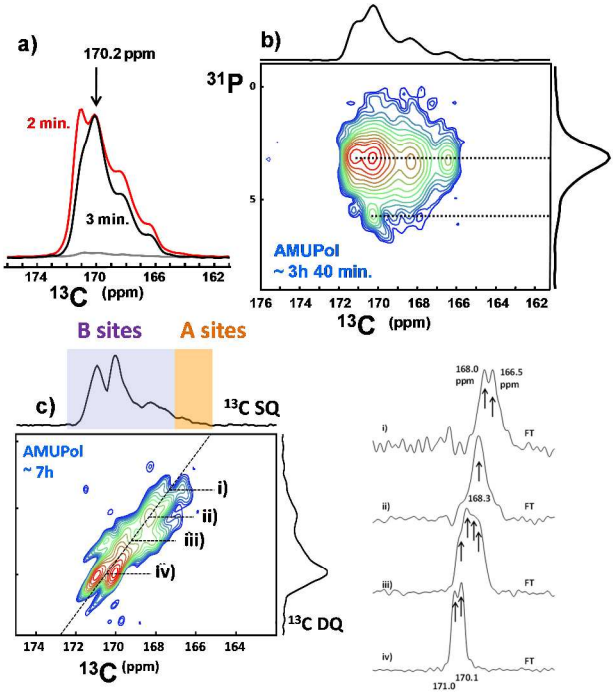

FIGURE 4

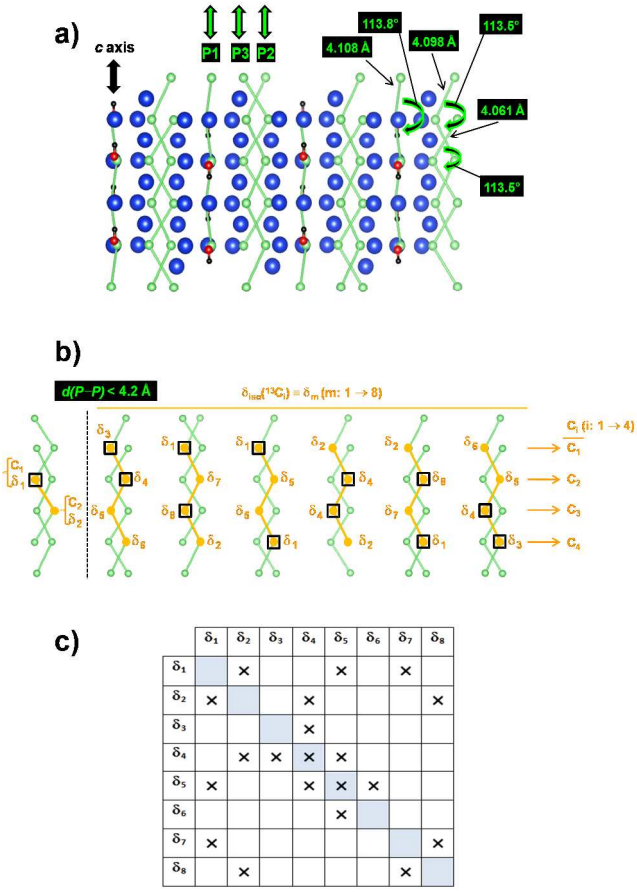

ASSOCIATED CONTENT

Supporting information: spin diffusion (SD) in HAp: modeling and orders of magnitude, TEM pictures of CHAp and *n.a.*CHAp, 2D $^{1}H \rightarrow {}^{31}P$ HETCOR CP MAS spectra of CHAp obtained at room temperature (RT), $^{1}H \rightarrow {}^{13}C$ CP MAS spectra of CHAp at room temperature (700 MHz) and T ~ 100 K (400 MHz), $^{1}H \rightarrow {}^{13}C$ CP MAS dynamics for CHAp at room temperature (300 MHz) and T ~ 100 K (400 MHz), $^{1}H \rightarrow {}^{13}C$ CP MAS spectra at variable contact time for CHAp and $NaHCO_3$, $^{1}H \rightarrow {}^{31}P \rightarrow {}^{13}C$ DNP HETCOR CP MAS spectrum of *n.a.*CHAp, DNP DQ CP MAS SPC5 spectrum without any GB apodization on both dimensions (2D-FT plot), other B/B associations in the (ab) plane and potential dipolar truncation, powder XDR and FTIR data for CHAp and *n.a.*CHAp. This material is available free of charge via the Internet at http://pubs.acs.org.

AUTHOR INFORMATION

Corresponding Author

* **Christian BONHOMME** (christian.bonhomme@upmc.fr)

Author Contributions

F.B., C.B., A.O. and S.H. initiated the work. C.C.-D, C.L., F.A., F.B. and C.B. performed the spectroscopic studies; L.B.-C., A.O. and S.H. performed the synthesis and first characterizations of the CHAp nanoparticles; the paper was mainly written by C.B.

Notes

The authors declare no competing financial interests.

ACKNOWLEDGMENT

The French Région Ile de France SESAME program is acknowledged for financial support (700 MHz spectrometer). C. Crevant is warmly acknowledged for early preparation of some of the samples studied in this contribution.

REFERENCES

Table of Contents artwork

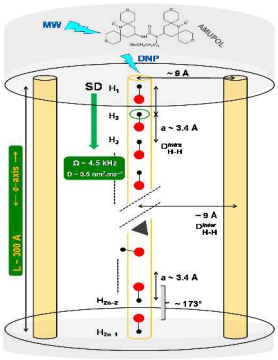

[1]. Elliott, J.C. *Reviews in Mineralogy and Geochemistry* **2002**, *48*, 427-453.

[2]. *Carbonated hydroxyapatite*, Fleet, M., Pan Stanford Publishing, 2015.

[3]. Finkemeier, C.G. *J. Bone Joint Surg. Am*. **2002**, *84*, 454-464.

[4]. Leventouri, T. *Biomaterials* **200**6, *27*, 3339-3342.

[5]. Wilson, R.M.; Elliott, J.C.; Dowker, S.E.P.; Smith, R.I. *Biomaterials* **2004**, *25*, 2205-2213.

[6]. Supova, M. *Ceramics International* **2015**, *41*, 9203-9231.

[7]. Ren, F.; Ding, Y.; Leng, Y. *J. Biomed. Mater. Res. Part A* **2014**, *102*, 496-505.

[8]. Yesinowski, J.P.; Eckert, H. *J. Am. Chem. Soc.* **1987**, *109*, 6274-6282.

[9]. Cho, G.; Wu, Y.; Ackerman, J.L. *Science* **2003**, *300*, 1123-1127.

[10]. Jäger, C.; Welzel, T.; Meyer-Zaika; W.; Epple, M. *Magn. Reson. Chem*. **2006**, *44*, 573-580.

[11]. Ben Osman, M.; Diallo-Garcia; S.; Herledan, V.; Brouri, D.; Yoshioka ; Kubo, J.; Millot, Y.; Costentin, G. *J. Phys. Chem. C* **2015***, 119*, 23008-23020.

[12]. McElderry, J.-D.P.; Zhu, P.; Mroue, K.H.; Xu, J.; Pavan, B.; Fang, M.; Zhao, G. McNerny, E.; Kohn, D.H.; Franceschi, R.T. *et al*. *J. Solid State Chem*. **2013**, *206*, 192-198.

[13]. Wang, Y. ; Von Euw, S. ; Fernandes, F.M. ; Cassaignon, S. ; Selmane, M. ; Laurent, G. ; Pehau-Arnaudet, G. ; Coelho, C. ; Bonhomme-Coury, L. ; Giraud-Guille, M.M. *et al*. *Nature Mater*. **2013**, *12*, 1144-1153.

[14]. Wise, E.R.; Maltsev; S. Davies ; M.E., Duer, M. ; Jaeger C. ; Loveridge, N., Murray, R.C.; Reid, D.G. *Chem. Mater*. **2007**, *19*, 5055-5057.

[15]. Reid, D.G.; Duer. M.J.; Murray, R.C.; Wise E.R. *Chem. Mater* **2008**, *20*, 3549-3950.

[16]. Beshah, K.; Rey, C.; Glimcher, M.J.; Shimizu, M., Griffin, R.G. *J. Solid State Chem.* **1990**, *84*, 71-81.

[17]. Mason, H.E.; Kozlowski, A.; Phillips, B.L. *Chem. Mater*. **2008**, *20*, 294-302.

[18]. Maly, T.; Debelouchina, G.T.; Bajaj, V.S.; Hu, K.-N.; Joo, C.-G.; Mak-Jurkauskas, L.; Sirigini, J.R.; van der Wel, J.R.S.; Herzfeld, J.; Temkin, R.J.; Griffin, R.G. *J. Chem. Phys*. **2008**, *128*, 052211-1-19.

[19]. Song, C.; Hu, K.-N.; Joo, C.-G.; Swager, T. M.; Griffin, R.G. TOTAPOL *J. Am. Chem. Soc.*, **2006**, *128*, 11385-11390.

[20]. Sauvée, C. ; Rosay, M. ; Casano, G. ; Aussenac, F. ; Weber, R. T.; Ouari, O.; Tordo, P. *Angew. Chem. Int. Ed.* **2013**, *52*, 10858-10861.

[21]. Lesage, A.; Lelli, M.; Gajan, D.; Caporini, M. A.; Vitzthum, V.; Mieville, P.; Alauzun, J.; Roussey, A.; Thieuleux, C. Mehdi, A. *et al. J. Am. Chem. Soc.* **2010**, *132*, 15459–15461.

[22]. Gelis, I. ;Vitzhum, V. ; Dhimole, N. ; Caporini, M. A. ; Schedlbauer, A.; Carnevale, D.; Connel, S.R. ; Fucini, P. ; Bodenhausen, G. *J. Biomol. NMR* **2013**, 56, 85-93.

[23]. Rossini, A.J. ; Zagdoun, A. ; Lelli, M. ; Lesage, A. ; Copéret, C. ; Emsley, L. *Acc. Chem. Res*. **2013**, *46*, 1942-1951.

[24]. Hirsh, D.A.; Rossini, A.J.; Emsley, L.; Schurko, R.W. *Phys. Chem. Chem. Phys*. **2016**, *18*, 25893-25904.

[25]. Baudouin, D.; van Kalkeren, H.; Bornet, A.; Vuichoud, B.; Veyre, L., Cavailles, M.; Schwarzwalder, M.; Liao, C.; Gajan, D., Bodenhausen, G. *et al. Chem. Sci*. **2016**, *7*, 6846-6850.

[26]. Chaudhari, S.R.; Berruyer, P.; Gajan, D.; Reiter, C.; Engelke, F.; Silverio, D.L.; Copéret, C.; Lelli, M.; Lesage, A.; Emsley, L. *Phys. Chem. Chem. Phys*. **2016**, *18*, 10616-10622.

[27]. Thankamony, L.A.S.; Lion, C.; Pourpoint, F.; Singh, B.; Perez Linde, A.J.; Carnevale, D.; Bodenhausen, G.; Vezin, H.; Lafon, O.; Polshettiwar, V. *et al. Angew. Chem. Int. Ed*. 2015, *54*, 2190-2193.

[28]. Lafon, O.; Rosay, M. ; Aussenac, F. ; Lu, X. ; Trébosc, J. ; Cristini, O. ; Kinowski, C. ; Touati, N. ; Vezin, H. ; Amoureux, J.P. *Angew. Chem. Int. Ed*. **2011**, *50*, 8367-8370.

[29]. Kobayashi, T. ; Perras, F.A. ; Wei Goh, T. ; Metz, T. L.; Huang, W. ; Pruski, M. *J. Phys. Chem. Lett*. **2016**, *7*, 2322-2327.

[30].Takahashi, H.; Viverge, B.; Lee, D.; Rannou, P.; De Paëpe, G. *Angew. Chem. Int. Ed*. **2013**, *52*, 6979-6982.

[31]. Lee, D. ; Bouleau, E. ; Saint-Bonnet, P. ; Hediger, S. ; De Paëpe, G. *J. Magn. Reson*. **2016**, *264*, 116-124.

[32]. Lee, D.; Hediger, S.; De Paëpe, G. *Solid State NMR* **2015**, *66-67*, 6-20.

[33]. Blanc, F.; Sperrin, L.; Jefferson, D.A.; Pawsey, S.; Rosay, Grey, C.P. *J. Am. Chem. Soc*. **2013**, *135*, 2975-2978.

[34]. Le, D. ; Ziarelli, F. ; Phan, T.N.T. ; Mollica, G. ; Thureau, P.; Aussenac, F. ; Ouari, O. ; Gigmes, D. ; Tordo, P. ; Viel, S. *Macromol. Rapid Comm.* **2015**, *36*, 1416-1421.

[35]. Ouari, O. ; Phan, T. ; Ziarelli, F. ; Casano, G. ; Aussenac, F. ; Thureau, P. ; Gigmes, D. ; Tordo, P. ; Viel, S. *ACS Macro Lett*. **2013**, *2*, 715-719.

[36] . Lee, D. ; Leroy, C. ; Crevant, C. ; Bonhomme-Coury ; L., F. Babonneau ; Laurencin, D. ; Bonhomme, C. ; De Paëpe, G. *Nature Commun*., **2017**, *8*, 14104 (2017).

[37]. Fleet, M.E.; Liu, X. *Am. Miner*. **2011**, *96*, 1148-1157.

[38]. Peroos, S.; Du, Z.; de Leeuw, N. H. *Biomaterials* **200**6, *27*, 2150-2161.

[39]. Astala, R. ; Stott, M.J. *Chem. Mater*. **2005**, *17*, 4125-4133.

[40]. Ulian, G.; Valdre, G.; Corno, M.; Ugliengo, P. *Am. Miner*. **2014**, *99*, 117-127.

[41]. van der Wel, P. C. A., Hu, K.-N., Lewandowski, Griffin, R. G. *J. Am. Chem. Soc*., **2006**, 128, 10840-10846.

[42]. Rossini, A.J.; Widdifield, C.M.; Zagdoun, A.; Lelli, M.; Schwaezwälder, M.; Copéret, C.; Lesage, A.; Emsley, L. *J. Am. Chem. Soc*. **2014**, 136, 2324-2334.

[43] Rossini, A. J.; Zagdoun, A.; Hegner, F. S.; Schwarzwälder, M.; Gajan, D.; Copéret, C.; Lesage, A.; Emsley, L. J. Am. Chem. Soc. 2012, 134, 16899−16908.

[44] Lafon, O.; Thankamony, A. S. L.; Kobayashi, T.; Carnevale, D.; Vitzthum, V.; Slowing, II; Kandel, K.; Vezin, H.; Amoureux, J. P.; Bodenhausen, G.; Pruski, M. J. Phys. Chem. C 2013, 117, 1375-1382.

[45] Multidimensional solid-state NMR and Polymers, Schmidt-Rohr, K. & Spiess, H.W., Academic Press, 1994.

[46]. Hohwy, M.; Rienstra, C.M.; Jaroniec, C.P.; Griffin, R.G. *J. Chem. Phys*. **1999**, *110*, 7983-7992.

[47]. Babonneau, F.; Bonhomme, C.; Hayakawa, S.; Osaka, A. MRS Proceedings, Fall Meeting, Boston, e-paper, 0984-MM06-05 (2007).

[48]. Metz, G.; Wu, X.L.; Smith, S.O. *J. Magn. Reson. A* **1994**, *110*, 219-227.

[49]. Fung, B.M.; Khitrin, A.; Ermolaev, K. *J. Magn. Reson*. **2000**, *142*, 97-101.

[50]. Coelho, C.; Rocha, J.; Madhu, P. K.; Mafra, L. *J. Magn. Reson*. **2008**, *194*, 264-282.